



Mg_{0.5}Zn_{0.5}Fe₂O₄-polyurethane thin nanocomposite coating as broadband microwave absorber

Rajarshi Bhattacharyya^{1,5} · Somnath Roy² · Om Prakash³ · Akhilendra Pratap Singh⁴ · Tapas Kumar Bhattacharya⁵ · Pralay Maiti³ · Somak Bhattacharyya⁴ · Santanu Das¹

© Springer Nature Switzerland AG 2018

Abstract

We report the synthesis of Mg_{0.5}Zn_{0.5}Fe₂O₄ (MZF) nanoparticles by gel combustion technique followed by fabrication of thin layer (~ 100 μm) of ferrite–polymer nanocomposite on aluminum substrate and its application on broadband absorption properties over the microwave frequency range of 4–15 GHz. The particle size of ferrite powder was controlled by changing citrate to nitrate molar ratios of precursors, which exhibit different adiabatic isotherms. XRD analysis showed that ferrite phase formation occurred for all systems and the system with lowest crystallite size (~ 30 nm) was obtained for the stoichiometric citrate to nitrate molar ratio. The nanocomposite coating showed excellent broadband absorption properties with absorptivity greater than 88%. This implied that the real and imaginary part of the surface impedance values of the nanocomposite coatings are close to 377 Ω and 0 Ω respectively, which is impedance of free space over the significant region of the frequency band of interest. The stoichiometric fuel based MZF of smallest average particle size showed best microwave absorption properties. The as-developed MZF nanocomposite coating showed minimum reflection from the coating over this frequency band, which can solve various electromagnetic interference issues, stealth technology, and the radiated EMI management in on board spacecraft and several others.

Keywords Magnesium zinc ferrites · Polyurethane · Nanocomposite coatings · Particle size · Broadband microwave absorption

1 Introduction

The accelerated increase in electromagnetic interference (EMI) has received a serious consideration from researchers who responded by producing a variety of radar absorbing materials (RAMs) especially at the GHz frequency ranges [1]. The performance of electromagnetic shielding and RAM depends on various newly emerging materials, which can efficiently absorb electromagnetic waves over a broad

range of frequencies. Recently, extensive researches on microwave frequency absorption properties of materials have been performed to achieve the best radar absorbing materials (RAM) with extraordinary absorptive ability and broadband absorption [2, 3]. Indeed, much attention has also been paid to nanoparticle based RAMs due to their exclusive microwave-energy absorption capability with effective diminution of electro-magnetic backscattering such that they are expected to have assuring applications

Electronic supplementary material The online version of this article (<https://doi.org/10.1007/s42452-018-0041-8>) contains supplementary material, which is available to authorized users.

✉ Santanu Das, santanudas.cer@iitbhu.ac.in | ¹Department of Ceramic Engineering, Indian Institute of Technology (BHU), Varanasi, Uttar Pradesh 221005, India. ²Department of Physics, Institute of Science, Banaras Hindu University, Varanasi, Uttar Pradesh 221005, India. ³School of Materials Science and Technology, Indian Institute of Technology (BHU), Varanasi, Uttar Pradesh 221005, India. ⁴Department of Electronics Engineering, Indian Institute of Technology (BHU), Varanasi, Uttar Pradesh 221005, India. ⁵Department of Ceramic Technology, Government College of Engineering and Ceramic Technology, Kolkata, West Bengal 700010, India.

SN Applied Sciences (2019) 1:38 | <https://doi.org/10.1007/s42452-018-0041-8>

Received: 11 August 2018 / Accepted: 30 October 2018 / Published online: 9 November 2018

in the stealth technology of military air-crafts, naval-ships, television image interference due to high-rise buildings, and the radiated EMI management in onboard spacecraft [4–6]. Microwave absorbers of different finite shapes fabricated from high-resistivity semiconductor materials are commonly used for this purpose. Although bulk materials are suitable for stationary applications (anechoic chambers for antenna measurements, echo rejecting systems, attenuators etc.), however, those are not fit for any moving objects. Therefore, a lightweight smooth surface in the form of microwave absorbing coating on metallic surface is the prerequisite for moving objects [7]. Metasurface-based structures have also been proposed for absorber applications, however, they cannot cover broad frequency band owing to their high “Q” value [8].

Ceramic ferrites or spinel ferrites are ferrimagnetic oxides, which exhibit general molecular formula $M^{2+}Fe_2^{3+}O_4^{2-}$, where divalent and trivalent metal cations like M^{2+} and Fe^{3+} occupy tetrahedral (A) and octahedral (B) sites, respectively. Soft ceramic ferrites show tremendous potential for applications as broadband microwave absorbing materials where saturation magnetization, anisotropy constants, Neel temperature, coercivity, remnant magnetization and the permeability play major role in absorption [9, 10]. In particular, the bond length and bond angle influence the super exchange interactions, which further results in effectively controlling the magnetization and coercivity by substituting different size ions in ferrites [11]. In addition, nano-sized ferrite particles have wide advantages including, size-dependent magnetic properties, the easy dispersibility, and high absorptivity at the GHz frequency range [12–14]. Materials are typically known as hybrid absorbers when the magnetic and electric fields attenuate simultaneously [15, 16]. To date, nanomaterials such as Cu–Zn, Mn–Zn, Ni–Zn, and other substituted soft-ferrites have been investigated for the application in radar wave absorbers [17–19]. Zn substituted ferrites show enhanced magnetic properties, which are particularly useful for high frequency applications. In this regard, magnesium zinc ferrites ($Mg_{1-x}Zn_xFe_2O_4$, $x=0.1-0.6$) is widely used materials for applications in telecommunication, power transformers, and ferrite cores owing to its low coercivity, high resistivity, and effectively low eddy current losses make it an excellent soft-magnetic material [20]. Although various methods like spray drying, freeze drying, co-precipitation and sol–gel are used for synthesizing ferrite nanoparticles, however, combustion synthesis is one of the low cost and rapid methods of synthesizing ultra-fine ferrite powders with controllable particle size. The type of fuel used, fuel to oxidizer ratio, ignition temperature and initial water content of the solution play vital role in controlling the final product of combustion synthesis of as discusses elsewhere [20, 21].

Primarily, the citrate (C) to nitrate (N) ratio influence the flame temperature, combustion rate, thus, affecting the morphology and particle size of the ferrite powder produced via this method. The electromagnetic absorption capabilities of materials are varied mostly on the nature, shape, and size of absorber materials [22, 23]. Furthermore, ferrite nanoparticles dispersed in polymer matrix forms a nanocomposite coating, which could have added advantage as sprayable coating for EMI shielding applications [24–26]. Several works have been demonstrated on polymer-based composites added with some magnetic filler materials, such as barium–ferrite [27], carbon materials like iron–fiber [28], Ni/Zn-ferrite [29] and Fe_3O_4 /yttrium iron garnet (YIG) [30]. Kong et al. reported the magnetic, electromagnetic and microwave absorbing properties of polymer-based nanocomposites consisting of thermoplastic natural rubber (TPNR) as the matrix and Fe_3O_4 nanoparticles as the fillers [31]. Therefore, the combination of polymers and nanomaterials is able to integrate the large electric/magnetic loss of nano-ferrites and the easy tenability of polymer and is possibly an optimal strategy to design excellent EM-wave absorption materials [32]. Zhao et al. [33] demonstrated the electromagnetic wave absorbing properties of amorphous carbon nanotubes/PVC (ACNT/PVC) composite films and found that the reflection loss below – 10 dB could be increased from 3.3 to 5.8 GHz, and the position of absorbing peak shifted from 12.96 to 14.44 GHz. Yang et al. demonstrated the size dependent Fe_3O_4 nanodisc for electromagnetic absorption properties where smaller nanodiscs exhibit better microwave absorption properties [34]. However, there are no reports on the controlled synthesis of $Mg_{0.5}Zn_{0.5}Fe_2O_4$ by varying the C/N ratio and its effect on the formation of varying particle size. Similarly, the effect of size dependent microwave absorption properties of magnetic nanoparticle in the GHz range is overlooked till date.

In this work, we demonstrate the synthesis of zinc substituted magnesium based spinel ferrite $Mg_{0.5}Zn_{0.5}Fe_2O_4$ (MZF) nanoparticles by varying amount of citrate–nitrate ratios (C/N ratios). By varying the amount of C/N ratios, our objective was to produce MZF nanoparticles with different particle size. Furthermore, our goal was to analyze the size-dependent magnetic properties, which might have a direct correlation to the microwave absorption properties of those nano-size ferrite particles. The final aim was to explore the microwave absorption properties (GHz range, from 4 to 15 GHz) of the nanocomposite coating prepared by the size dependent MZF-polyurethane coating on the metal substrate. Furthermore, we have investigated the broadband microwave absorption properties of nanocomposite coatings via free-space measurement technique. This work would have potential in various other microwave applications, including, radar absorbing materials

(RAM), radiation absorption for stealth technology, EMI shielding of any electromagnetically interfering devices, and radiation absorption for sensor-technologies.

2 Experimental

2.1 Materials

Chemical grade Magnesium (II) nitrate hexahydrate $[\text{Mg}(\text{NO}_3)_2 \cdot 6\text{H}_2\text{O}]$ and iron (III) nitrate nonahydrate $[\text{Fe}(\text{NO}_3)_3 \cdot 9\text{H}_2\text{O}]$, Zinc (II) nitrate $[\text{Zn}(\text{NO}_3)_2 \cdot 6\text{H}_2\text{O}]$, citric acid anhydrous and ammonia solution (both are 99.9% pure, purchased from Merck, Germany) were used as starting materials for synthesis of $\text{Mg}_{0.5}\text{Zn}_{0.5}\text{Fe}_2\text{O}_4$ powder without any further purification.

2.2 Synthesis of $\text{Mg}_{0.5}\text{Zn}_{0.5}\text{Fe}_2\text{O}_4$ powder

The nitrate precursors were dissolved in minimum amount of deionised water in the desired molar ratio, citric acid was then added with constant stirring by adjusting different citrate to nitrate molar ratio. The solution was heated in atmospheric conditions on a hot plate at 80 °C until gelation took place. It was allowed to ignite by further raising the temperature and a fluffy brown mass was formed with evolution of large volumes of gases. The combustion product was then heat treated at about 800 °C for 2 h.

2.3 Fabrication of nanocomposite coating

Thermoplast polyurethane (TPU) was obtained from Bayer Material Science AG: polyester based TPU (Desmopan 385S) having the shore hardness of 86A. This polymer was very similar to the materials used for conventional paints for various surface coating [35]. TPU and different MZF nanoparticles were taken in 1:1 weight ratio for nanocomposite fabrication. First, TPU was dissolved in dimethylformamide (DMF) by stirring it at 100 °C followed by addition of ferrite nanoparticles in the solution. The solution mixture was kept under high power probe sonicator for

15 min and transferred to the hot plate (100 °C). The Al substrate (dimension: 152 mm × 152 mm × 0.875 mm) was coated by simple hand brushing with the as-prepared nanocomposite solution as shown in Fig. 1a. The coated samples were tested under standard free-space absorption measurement set-up as schematically illustrated in Fig. 1b. The step-by-step measurements of different nanocomposite coated samples are also illustrated in Fig. S3 (Supporting Information).

2.4 Characterization of $\text{Mg}_{0.5}\text{Zn}_{0.5}\text{Fe}_2\text{O}_4$ powder

2.4.1 X-ray diffraction analysis

Structural and phase analysis of as synthesized Mg–Zn ferrite powder was carried out in an X-ray diffraction (XRD) (Rigaku, Japan) analysis instrument. The diffraction peaks were identified using JCPDS data 01-088-1942. The diffraction peaks show the characteristics of pure phase spinel structure with most intense reflection from the (311) plane.

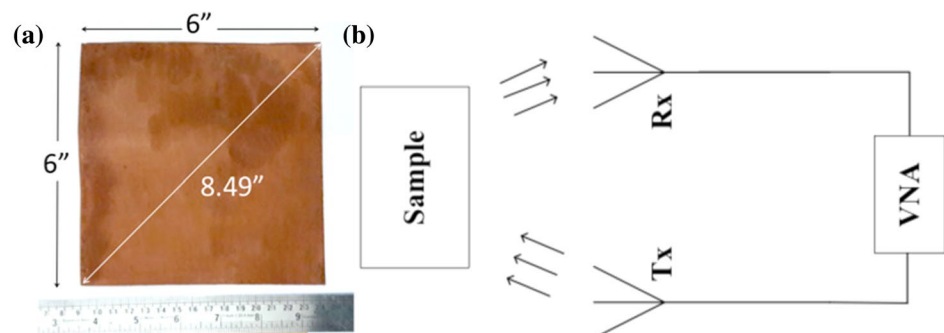
2.4.2 Transmission electron microscopy

The particle size and morphology of the as prepared Mg–Zn Ferrite powder and Mg–Zn Ferrite–polyurethane (PU) nanocomposites were characterized using a transmission electron microscope (TECNAI G2 20 TWIN, FEI, USA). All the samples (both MZF nanoparticles and MZF-PU) were dispersed in methanol followed by drop casting onto a coated TEM grid. All the results, including, TEM/HRTEM and selected area electron diffraction (SAED) patterns of all the samples were collected under 200 kV acceleration voltage.

2.4.3 Measurement of magnetic properties

Magnetic properties of the samples were measured using a vibrating sample magnetometer (VSM) (Model: EZ9, Microsense, USA). First, the powder sample was filled in an acrylic cup and then the entire assembly was fixed to

Fig. 1 **a** Photograph showing the Mg–Zn ferrite coated Aluminium substrate of diagonal distance ~8.5 inch; **b** schematic diagram for measuring reflection coefficients (S_{11}) for samples using a pair of identical antennas connected to vector network analyzer



quartz rods for mounting onto the VSM. The samples were first AC demagnetized with a demagnetizing factor of 0.9 followed by the M–H measurements. The respective background corrections were done with the same measurement conditions for each sample.

2.4.4 Measurement of broadband microwave properties

Free space measurement was carried out to characterize the reflection and transmission coefficients of the MZF-polymer structures, while the transmission through a thin coating has been measured using this method reported elsewhere [36, 37]. For measuring the absorptivity of the sample, the as fabricated device (described in the Sect. 2.3) was kept within the anechoic chamber. Three different pairs of horn antennas in C-band, X-band and Ku-band have been used separately for the measurement of reflection from the fabricated structure. Each of the pairs of horn antennas was identical and one of them was used as transmitter to launch the electromagnetic wave onto the sample while the other one was used to receive the reflection from the sample. The horn antennas were connected to the vector network analyzer (Anritsu MS 2037, Japan). Initially, a reflection profile was recorded from the surface of pure Al-substrate without any coating, which was considered as reference value as the metal plate behaves as an ideal reflector [38]. Thereafter, the reflection coefficients were measured from the samples to compute the actual reflection loss for different samples, which in turn could provide the evaluation of absorptivity. The step-by-step measuring techniques are schematically shown in Fig. S3 (Supporting information).

3 Results and discussion

We synthesized Magnesium Zinc Ferrite ($Mg_{0.5}Zn_{0.5}Fe_2O_4$) using gel combustion technique and we have changed the citrate to nitrate molar ratio in order to control the particle size and phase formation in the ferrites shown in Table 1. Figure 2 shows the XRD patterns of $Mg_{0.5}Zn_{0.5}Fe_2O_4$ (MZF) nano powders synthesized with varying citrate to nitrate

Table 1 Shows the particle size and the crystal lattice parameters of the various MZF samples prepared with various thermodynamic conditions

Sample	Average crystallite size (nm)	Lattice parameter (Å)
MZFD (C/N = 0.22)	45 ± 4	8.405
MZFS (C/N = 0.2775)	30 ± 8	8.418
MZFE (C/N = 0.33)	55 ± 7	8.418

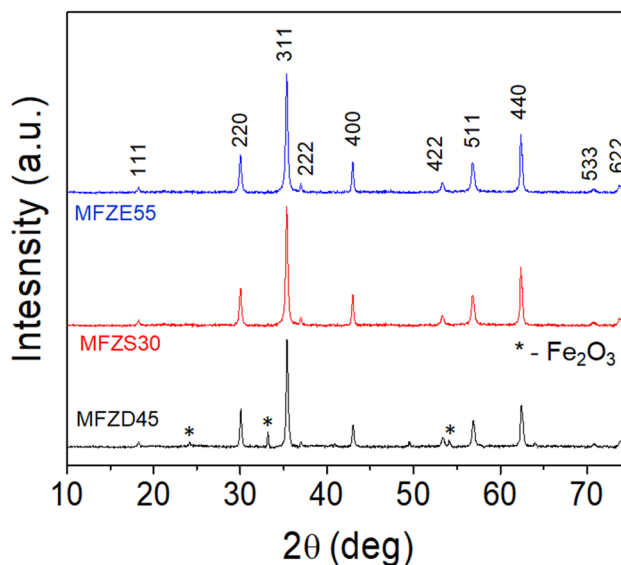


Fig. 2 Show the x-ray diffraction results of various MZF samples with various particle sizes

molar ratio and the various XRD peaks are identified using the standard line profile JCPDS data (No 01-088-1942). The diffraction peaks of fuel rich (C/N = 0.33) sample and stoichiometric fuel sample (C/N = 0.2775) show the characteristic reflections for pure phase spinel structure with the most intense reflection from the plane (311). Thus, the as synthesized MZF ferrites exhibit cubic structure with $Fd3m$ space group. The fuel deficient (C/N = 0.22) sample shows weakly intense diffraction peaks of Fe_2O_3 along with spinel phase ferrite indicating the presence of impurities and can be attributed to the fact that it undergoes incomplete combustion thus lacking sufficient energy for pure phase formation. The average crystallite size from XRD data was calculated using the Debye–Scherrer equation and listed in the Table 1 with corresponding lattice parameters of the various MZF samples. It could be seen from Table 1 that the MZF produced with stoichiometric fuel ratio is the lowest among all the samples. However, the average particle size of the MZF produced using fuel deficient process and the MZF produced using fuel excess process exhibits higher particle size of 45 nm and 55 nm, respectively. This further manifests that the thermodynamics and kinetics of the nucleation and growth of MZF particles solely depends on the fuel to oxidizer molar ratio. The further details on the thermodynamic parameters and the calculations regarding the adiabatic flame temperature of the size-controlled ferrite particle formation are given in Sect. S1 (Supporting information). These various nano-sized MZF particles showed varied magnetic properties hence exhibited various level of microwave absorption as discussed in the later section of this manuscript. For the convenience and

easy understanding of various interdisciplinary readers, the name of the MZF samples, such as, MZF (C/N=0.22), MZF (C/N=0.2775), and MZF (C/N=0.33) of particle size of 45 nm, 30 nm and 55 nm will be addressed as MZFD45, MZFS30 and MZFE55, respectively, throughout the rest of the manuscript.

The MZFS30 sample with lowest average particle size was characterized under TEM/HRTEM to identify its structure, morphology and phase formation. In addition, we have dispersed the same MZFS30 particles in TPU and transfer it over TEM grid in order to check the particle dispersion and the ferrite/polymer interface formation under the best optimized condition. TEM images in Fig. 3 showed that non uniform shape and sizes of MZF30 particle with irregular surface morphology. The MZF30 also shows lowest average particle size of ~30 nm which is pretty closely aligned with the data obtained from XRD.

Figure 3a, b demonstrate the bright field (BF) images of MZF30 with different magnifications. Figure 3c illustrates the selected area electron diffraction (SAED) pattern of the MZF30 where ring-patterns depict the formation of polycrystalline $Mg_{0.5}Zn_{0.5}Fe_2O_4$ particles. The first four polycrystalline rings are representative of characteristics (111), (220), (311), and (222) planes, thus, demonstrate the formation of phase-pure $Mg_{0.5}Zn_{0.5}Fe_2O_4$. Figure 3d–f

show the similar MZF30 particles dispersed in PU matrix for nanocomposite formation. Figure 3d, e demonstrate the BF images with various magnifications where it is clearly observed that ferrite particles are clearly embedded inside of a polymer matrix. As could be seen from the Fig. 3e, a single-ferrite particle is surrounded with PU polymer which also suggested the homogeneous dispersion of the particles in the polymer matrix during the nanocomposite formation. Figure 3f show the SAED pattern of the MZF30-PU nanocomposite, which is exactly comparable to the Fig. 3c, suggests the phase-pure MZFS30 samples dispersed in TPU. Bright dots in the SAED pattern also manifests the occurrence of uniformly dispersed nanocrystalline MZF in PU. The SAED pattern for nanocomposite also exhibits the characteristics ferrite planes (similar to the Fig. 3c), hence indicate the homogeneous dispersion of the MZF30 powder in the polyurethane matrix.

Magnetic properties of the as-synthesized MZF are shown in Fig. 4 where magnetization (M) versus applied field (H) plot shows the slim hysteresis curve, which is indicative of soft-ferrimagnetic properties of MZF. It is clearly seen from the Fig. 4a that there is no significant difference in the magnetization values of the various MZF samples. This may be due to the broad distribution of the magnetic domains in the ferrites samples produced under

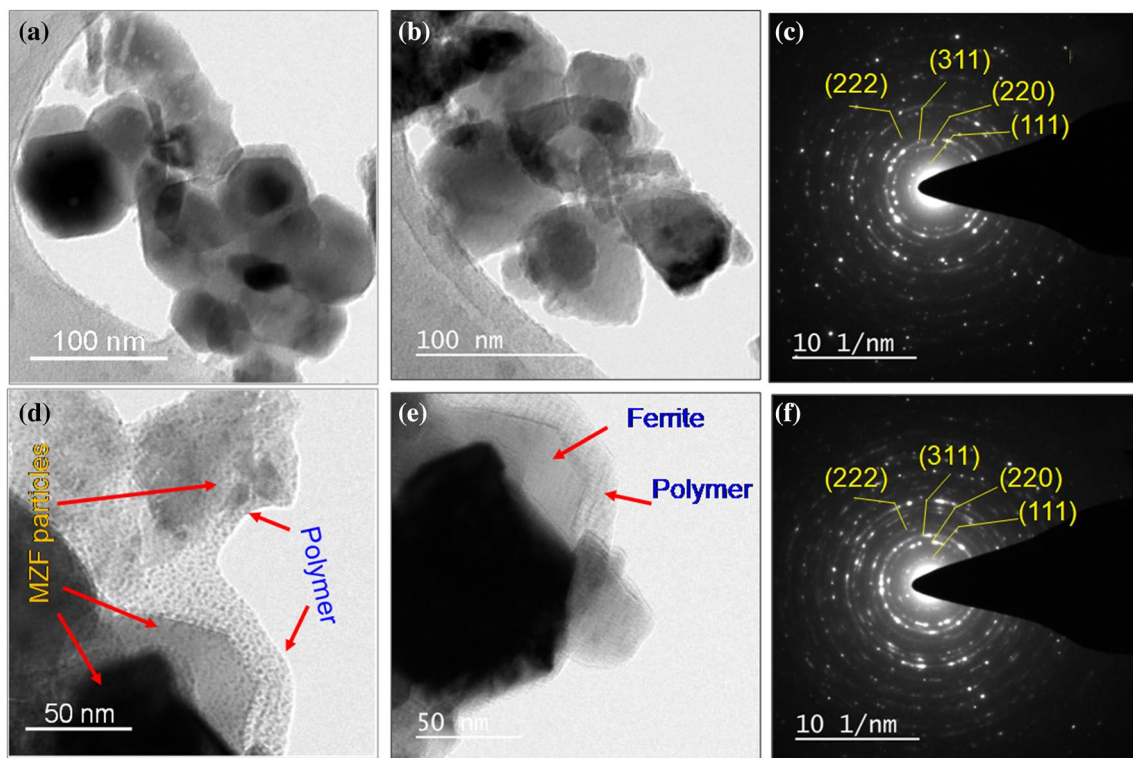


Fig. 3 Shows the transmission electron micrograph of **a** and **b** MZFS30 sample with various particle morphologies; **c** the SAED pattern of the MZF30 sample; **d** and **e** shows the MZFS30-PU

nanocomposite under different dispersion level showing the clear markings of single ferrite nanoparticles coated with polymer; **f** the SAED pattern of MGF-PU nanocomposite

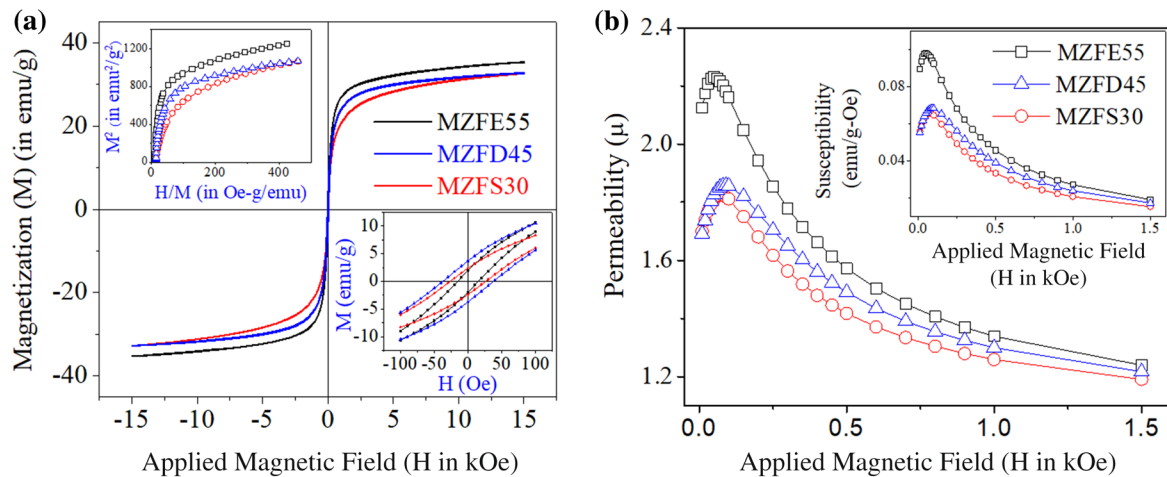


Fig. 4 a Shows the magnetization (M) versus applied magnetic field (H) curve of three different MZF samples with different average particle sizes; top inset shows the Arrot plot demonstrate the presence of magnetic orderings; the bottom inset showing the

various C/N ratios. The increase in saturation magnetization occurred with increase in MZF particle size and this may be due to the size dependent magnetic domain formation in the spinel ferrite materials. The size of the nanoparticles affects their magnetic properties. According to domain theory the smaller the crystal size, lower is the number of domains, which also tends to a single domain. This leads to the formation of smaller magnetic dipole moment, which results in a lower saturation magnetization and this can be clearly seen from the results presented in the manuscript. There is no significant changes found in the coercivity of those MZF samples with different particle size (Fig. 4a, lower inset) and this further suggested that all the MZF particles are soft-ferrimagnetic in nature. Figure 4a upper inset shows the Arrot plot where M^2 versus H/M plot depicts the magnetic orderings in the ferrimagnetic MZF particles. Figure 4b demonstrates the magnetic permeability (μ) versus magnetic field data of those three different samples of MZF with various particle sizes. Figure 4b inset shows the magnetic susceptibility (χ) of three MZF samples and found that MZFS30 exhibits lowest μ as well as lowest χ . As we know, the permeability of a material defines its ability to allow the magnetic lines of force to pass through it. It can be clearly seen from the Fig. 4b that the sample MZFS30 has the lowest permeability in the low field region compared to the others. This implies that any incident magnetic field on MZFS30 will be either reflected back or absorbed the most from the sample as compared to MZFE55 and MZFD45. Since the magnetic component of the incident microwaves have a very low magnitude, hence it can be considered to fall in this low field region. As such the MZFS30 should show the highest broadband

coercivity of the samples with different range of particle sizes **b** illustrates permeability versus applied field plots with various MZF samples with various particle size where the susceptibility versus applied field data shows at the inset of the figure

microwave absorptivity for the incident radiation in the GHz frequency range, which is quite well aligned with our broadband measurement data as discussed in the next section.

The as-prepared MZF-polymer coatings (as discussed in Sect. 2.3) under three distinct cases have been studied experimentally for reflection measurement. The measurement has been performed under free-space technique where the reflection from the sample has been measured using a pair of horn antennas. Three identical pair of horn antennas in C-band, X-band and Ku-band has been used for the measurement purpose. The antennas are connected to the Vector Network Analyzer Anritsu MS2038C where one of the antennas is used as transmitting antenna and the other as receiving antenna (Fig. 1b). The entire arrangement was kept within anechoic chamber to avoid all interferences from the outside. Initially, reflection has been measured by using an aluminum plate and PU coated aluminum plate of identical dimension. Similarly, the reflection measurement was also carried out from an aluminum plate coated with MZF-PU nanocomposite coatings. The step-by-step measurement procedure is demonstrated in Fig. S3 (Supporting information). The electromagnetic wave incident to the metal plate is behaving as complete reflector in this case as shown in Fig. S4 a (supportive information). On the other hand, the PU coated aluminum plate (PU/Al) exhibited as an ideal reflector (i.e. the absorbance was negligible) as shown in Fig. S4b (Supporting information). Thereafter, reflections from the MZF-PU nanocomposite surface were measured and found significantly different compared to the PU/Al surface. The difference between these two data will give rise to the actual reflection from the dispersed ferrite samples. The

similar procedures were performed for measuring reflection coefficient (S_{11}) for the other two samples (Fig. 5). The complete reflection data is shown in Fig. 5 and the comparisons of the reflections for all the three cases are shown in Fig. 6. Tiny nanometer dimension particle of MZF (i.e. 30 nm MZF particles), well dispersed in polyurethane matrix, has the maximum effect on S_{11} as opposed to the bigger dimension particle mostly clustered in PU matrix while the concentration of particles remains similar. Hence, well dispersed smaller dimension MZF has better efficacy towards S_{11} and thereby greater absorptivity of broadband frequency.

For all these MZF-PU nanocomposite structures, the surface impedance was calculated. This measured surface impedance is identical with the input impedance of a transmission line with characteristic impedance Z_0 [39]. The surface impedance has been calculated from the measured reflection coefficient using the Eq. 1. Here, the surface impedance Z_s has been computed from the measured reflection coefficient S_{11} and free space impedance Z_0 .

$$Z_s = Z_0 \frac{1 + S_{11}}{1 - S_{11}} \tag{1}$$

The variations of real and imaginary parts of surface impedance of the three distinct samples are shown in

Fig. 7. Here, the incident electromagnetic wave will be completely absorbed when the calculated surface impedance is exactly equal to the characteristic impedance of free space of 377Ω .

As seen from Fig. 7a, it is evident that the real and imaginary parts of calculated surface impedance are close to 377Ω and 0Ω respectively for the sample MZFD30. In order to achieve the minimum reflection from the sample surface ($S_{11} = 0$), the surface impedance should match with the free space impedance. Since the transmission is minimized due to aluminum coating on the backside of the sample, further minimizing the reflection from the sample ensures maximum absorption taken place within the sample. Thus, when the sample undergoes highest absorption close to 100%, real and imaginary parts of Z_s possess values close to 377Ω and 0Ω respectively, equal to the value of free space impedance. Considering the transmission is zero in all the three cases due to complete metallic backing, the best absorptivity is realized over broader frequency range for MZFS30 (Fig. 7a) with more than 85% absorptivity over the complete band. However, for MZFD45 and MZFE55 samples, the real and imaginary parts of Z_s exhibit values far away from 377Ω and 0Ω respectively, manifests the lower absorptivity as

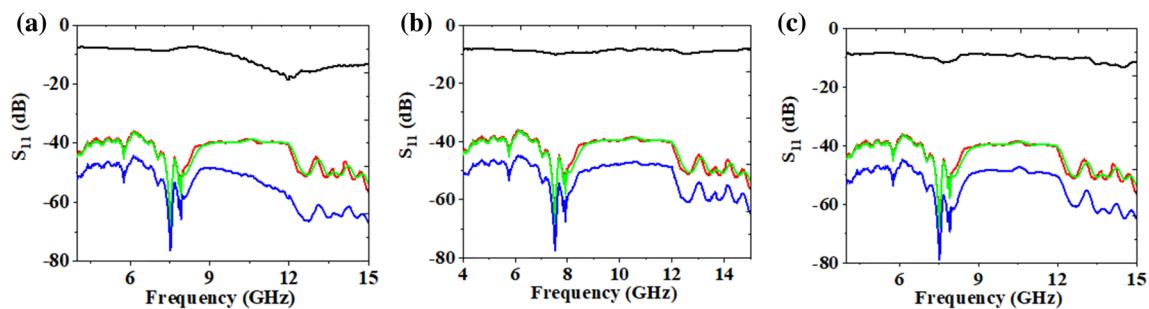
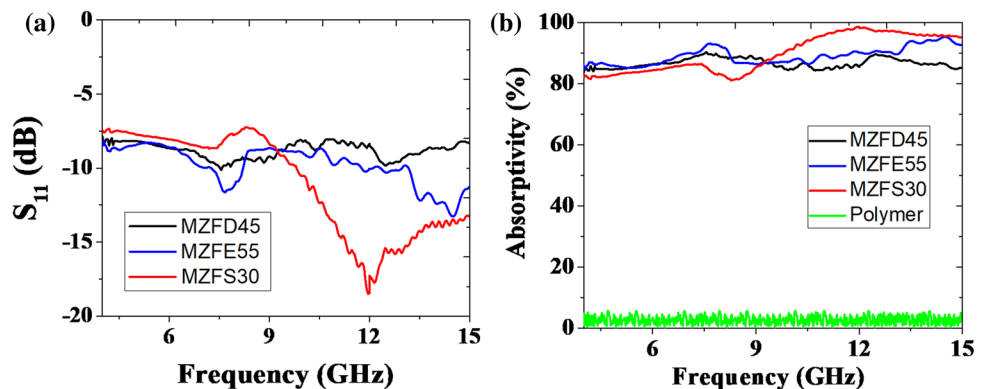


Fig. 5 Shows the reflection coefficients (S_{11}) from bare-metal surface (red line), polymer surface (green line), and MZF-polyurethane nanocomposite surface (blue line); the actual reflection coefficient

(black line on top) of the sample for each sample of **a** MZFS30, **b** MZFD45, and **c** MZFE55

Fig. 6 **a** Shows the variation of S_{11} with frequency for those three MZF samples; **b** demonstrate the variation of % microwave-absorptivity of those various MZF samples



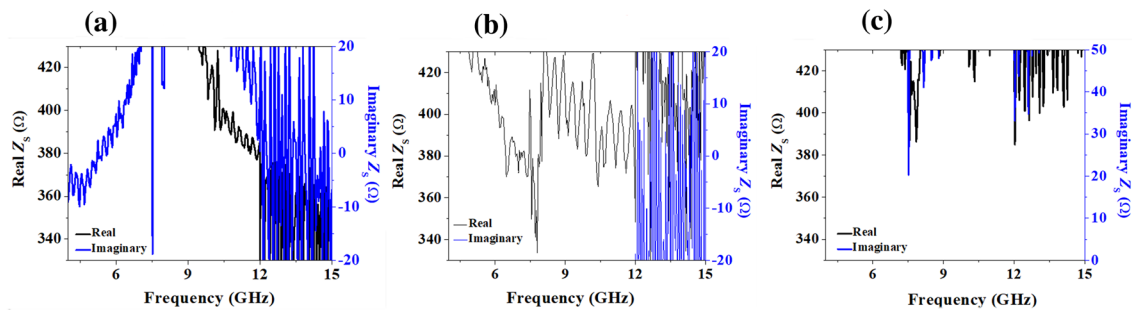


Fig. 7 Surface impedance shows the variation of real and imaginary Z_s with the frequency for **a** MZFS30, **b** MZFD45, and **c** MZFE55

demonstrated in Fig. 6. It is well known that the smaller the particle size greater is the surface area penetrated by the electromagnetic waves [40]. Magnetic dipoles, which result in the more active particles, are one of the properties of absorbing electromagnetic waves. The smaller particle size results in greater surface area and highest density, which affects higher microwave absorption. We believe that ferrite nanoparticles are highly susceptible to polarization under an electromagnetic field, thus, each nanoparticle can act as a center of electric dipole in electromagnetic field. Furthermore, these nanoparticles are again very susceptible to space charge polarization by trapping space charges and thereby enhancing the microwave properties [41, 42]. In addition, smaller the particle size, greater is the surface area, which are penetrated by the electromagnetic waves. In this context, the magnetic dipoles, which result in the more active particles, are one of the properties of absorbing electromagnetic waves. The smaller particle size results in greater surface area and highest density, which affects microwave absorption as demonstrated in this work.

In brief, we demonstrate the efficacy of the nanometer dimension ferrite towards the broadband frequency absorption by embedding the particle in polymer matrix for better processing and easy application as coating on metal surfaces. Furthermore, the nanocomposite coating was found to be lightweight, durable, sprayable, hence we believe it would have enormous possibilities for scalable industrial applications.

4 Conclusion

In conclusion, we have successfully demonstrated the size-dependent broadband absorption properties of $Mg_{0.5}Zn_{0.5}Fe_2O_4$ nanoparticles where the size of the ferrite particles and its dispersibility in a thermoplast polymer play an important role in the absorption properties. The sizes of the MZF particles are controlled by controlling the fuel ratios, which play key role in controlling

adiabatic isotherm of the gel-combustion reaction of the system. The phase-pure Mg–Zn ferrite with average lowest particles size of ~ 30 nm was obtained for stoichiometric fuel ratios while the average particle sizes were found to be higher for other two fuel ratios. The MZF particles showed size dependent magnetic properties, including, saturation magnetizations, coercivity, and susceptibility. The polymer nanocomposite coating showed excellent broadband absorption properties over the frequency range of 4–15 GHz with absorptivity greater than 85%. The real and imaginary components of the surface impedance values of the coatings are found to be 377Ω and 0Ω , respectively, over the significant region of the frequency band of interest. This implies minimum reflection from the coating over the frequency band of interest, thus, producing broadband absorption in the microwave frequency range. The MZF-polyurethane nanocomposite coatings on metal substrates will find enormous possibilities for application as materials in electromagnetic interference, electromagnetic shielding, stealth technology, and the radiated EMI management in onboard spacecraft etc.

Acknowledgements Authors gratefully acknowledge the support of Prof. A. K. Ghosh, Laboratory for Central Facilities, Department of Physics, Institute of Science, Banaras Hindu University, for extending the magnetic measurements facility. Also, authors are sincerely acknowledging the help of Prof. P. K. Jain, Department of Electronics Engineering, IIT (BHU) for extending his free-space measurement facilities. Authors are thankful to Prof. S. Chatterjee, Department of Physics, IIT (BHU) for some valuable discussion and suggestions on this work. Authors are highly grateful to Prof. K. Chakraborty, Principal, Govt. College of Engineering and Ceramic Technology for providing some facilities for this research work.

Funding This study was funded by Dr. Santanu Das's Seed Grant (Grant Number: IIT (BHU)/R&D/SM/2016-17/1238/L) provided by Indian Institute of Technology (BHU), Varanasi, India.

Compliance with ethical standards

Conflict of interest The authors declare that they have no conflict of interest.

References

1. Tang X, Hu K-A (2007) Preparation and electromagnetic wave absorption properties of Fe-doped zinc oxide coated barium ferrite composites. *Mater Sci Eng B* 139:119. <https://doi.org/10.1016/j.mseb.2007.01.052>
2. Kumar S, Meena RS, Chatterjee R (2016) Microwave absorption studies of Cr-doped Co-U type hexaferrites over 2–18 GHz frequency range. *J Magn Magn Mater* 418:194. <https://doi.org/10.1016/j.jmmm.2016.02.084>
3. Gairola SP, Verma V, Pandey V, Ravi, Purohit LP, Kotnala RK (2010) Modified composition of cobalt ferrite as microwave absorber in x-band frequencies. *Integr Ferroelectr* 119:151. <https://doi.org/10.1080/10584587.2010.503797>
4. Peng C-H, Hwang C-C, Wan J, Tsai J-S, Chen S-Y (2005) Microwave-absorbing characteristics for the composites of thermal-plastic polyurethane (TPU)-bonded NiZn-ferrites prepared by combustion synthesis method. *Mater Sci Eng, B* 117:27. <https://doi.org/10.1016/j.mseb.2004.10.022>
5. Shin JY, Oh JH (1993) The microwave absorbing phenomena of ferrite microwave absorbers. *IEEE Trans Magn* 29:3437. <https://doi.org/10.1109/20.281188>
6. Xu J-J, Yang C-M, Zou H-F et al (2009) Electromagnetic and microwave absorbing properties of Co₂Z-type hexaferrites doped with La³⁺. *J Magn Magn Mater* 321:3231. <https://doi.org/10.1016/j.jmmm.2009.05.039>
7. Liu Z-H, Tao R, Luo P, Shu X, Ban G-D (2017) Preparation and microwave absorbing property of carbon fiber/polyurethane radar absorbing coating. *RSC Adv* 7:46060. <https://doi.org/10.1039/c7ra07666e>
8. Munaga P, Ghosh S, Bhattacharyya S, Chaurasiya D, Srivastava KV (2015) An ultra-thin dual-band polarization-independent metamaterial absorber for EMI/EMC applications. In: 2015 9th European conference on antennas and propagation (EuCAP)
9. Naito Y, Suetake K (1971) Application of ferrite to electromagnetic wave absorber and its characteristics. *IEEE Trans Microw Theory Tech* 19:65. <https://doi.org/10.1109/TMTT.1971.1127446>
10. Tripathi KC, Abbas SM, Sharma RB, Alegaonkar PS, Verma M (2015) Microwave absorption studies of γ -ferrite & Ni-Zn ferrite/epoxy based nano composite. *Int J Sci Adv Res Technol* 1:16
11. Pardavi-Horvath M (2000) Microwave applications of soft ferrites. *J Magn Magn Mater* 215–216:171. [https://doi.org/10.1016/S0304-8853\(00\)00106-2](https://doi.org/10.1016/S0304-8853(00)00106-2)
12. Panwar R, Agarwala V, Singh D, Predeep P, Sujith A (2014) Design and experimental verification of a thin broadband nanocomposite multilayer microwave absorber using genetic algorithm based approach. *AIP Conf Proc* 1620:406. <https://doi.org/10.1063/1.4898273>
13. Kumar A, Agarwala V, Singh D (2013) Effect of particle size of BaFe₁₂O₁₉ on the microwave absorption characteristics in x-band. *Prog Electromagn Res M* 29:223
14. Rajendran M, Pullar RC, Bhattacharya AK, Das D, Chintalapudi SN, Majumdar CK (2001) Magnetic properties of nanocrystalline CoFe₂O₄ powders prepared at room temperature: variation with crystallite size. *J Magn Magn Mater* 232:71. [https://doi.org/10.1016/S0304-8853\(01\)00151-2](https://doi.org/10.1016/S0304-8853(01)00151-2)
15. Martins CR, Faez R, Rezende MC, De Paoli MA (2004) Microwave absorption properties of a conductive thermoplastic blend based on polyaniline. *Polym Bull* 51:321. <https://doi.org/10.1007/s00289-003-0223-3>
16. Martins CR, Faez R, Rezende MC, De Paoli MA (2006) Reactive processing and evaluation of butadiene–styrene copolymer/polyaniline conductive blends. *J Appl Polym Sci* 101:681. <https://doi.org/10.1002/app.23843>
17. Cho H-S, Kim S-S (2015) Design of grid-type microwave absorbers with high-permittivity composites of Ag-coated Ni-Zn ferrite particles. *J Appl Phys* 117:17A311. <https://doi.org/10.1063/1.4913645>
18. Li L, Chen X, Qi S (2016) Preparation and microwave absorbing property of Ni-Zn ferrite-coated hollow glass microspheres with polythiophene. *J Magn Magn Mater* 417:349. <https://doi.org/10.1016/j.jmmm.2016.05.101>
19. Zhao D-L, Lv Q, Shen Z-M (2009) Fabrication and microwave absorbing properties of Ni-Zn spinel ferrites. *J Alloy Compd* 480:634. <https://doi.org/10.1016/j.jallcom.2009.01.130>
20. Hajarpour S, Gheisari K, Honarbakhsh Raouf A (2013) Characterization of nanocrystalline Mg_{0.6}Zn_{0.4}Fe₂O₄ soft ferrites synthesized by glycine-nitrate combustion process. *J Magn Magn Mater* 329:165. <https://doi.org/10.1016/j.jmmm.2012.10.023>
21. Varma A, Mukasyan AS, Rogachev AS, Manukyan KV (2016) Solution combustion synthesis of nanoscale materials. *Chem Rev* 116:14493. <https://doi.org/10.1021/acs.chemrev.6b00279>
22. Xiang J, Li J, Zhang X, Ye Q, Xu J, Shen X (2014) Magnetic carbon nanofibers containing uniformly dispersed Fe/Co/Ni nanoparticles as stable and high-performance electromagnetic wave absorbers. *J Mater Chem A* 2:16905. <https://doi.org/10.1039/C4TA03732D>
23. Abdalla I, Shen J, Yu J, Li Z, Ding B (2018) Co₂O₄/carbon composite nanofibrous membrane enabled high-efficiency electromagnetic wave absorption. *Sci Rep* 8:12402. <https://doi.org/10.1038/s41598-018-30871-2>
24. Idris FM, Hashim M, Abbas Z, Ismail I, Nazlan R, Ibrahim IR (2016) Recent developments of smart electromagnetic absorbers based polymer-composites at gigahertz frequencies. *J Magn Magn Mater* 405:197. <https://doi.org/10.1016/j.jmmm.2015.12.070>
25. Ting TH, Yu RP, Jau YN (2011) Synthesis and microwave absorption characteristics of polyaniline/NiZn ferrite composites in 2–40 GHz. *Mater Chem Phys* 126:364. <https://doi.org/10.1016/j.matchemphys.2010.11.011>
26. Ali NN, Al-Marjeh RAQB, Atassi Y, Salloum A, Malki A, Jafarian M (2018) Design of lightweight broadband microwave absorbers in the X-band based on (polyaniline/MnNiZn ferrite) nanocomposites. *J Magn Magn Mater* 453:53. <https://doi.org/10.1016/j.jmmm.2018.01.014>
27. Li BW, Shen Y, Yue ZX, Nan CW (2007) Influence of particle size on electromagnetic behavior and microwave absorption properties of Z-type Ba-ferrite/polymer composites. *J Magn Magn Mater* 313:322. <https://doi.org/10.1016/j.jmmm.2007.01.017>
28. Wu M, He H, Zhao Z, Yao X (2000) Electromagnetic and microwave absorbing properties of iron fibre-epoxy resin composites. *J Phys D Appl Phys* 33:2398
29. Yusoff AN, Abdullah MH, Ahmad SH, Jusoh SF, Mansor AA, Hamid SAA (2002) Electromagnetic and absorption properties of some microwave absorbers. *J Appl Phys* 92:876. <https://doi.org/10.1063/1.1489092>
30. Yusoff AN, Sani JM, Abdullah MH, Ahmad SH, Ahmad N (2007) Electromagnetic and absorption properties of some TPNR/Fe₃O₄/YIG microwave absorbers as revealed by a microwave vector network analyser and specular absorber method. *Sains Malaysiana* 36:65
31. Kong I, Hj Ahmad S, Hj Abdullah M, Hui D, Nazlim Yusoff A, Puryanti D (2010) Magnetic and microwave absorbing properties of magnetite–thermoplastic natural rubber nanocomposites. *J Magn Magn Mater* 322:3401. <https://doi.org/10.1016/j.jmmm.2010.06.036>
32. Huo J, Wang L, Yu H (2009) Polymeric nanocomposites for electromagnetic wave absorption. *J Mater Sci* 44:3917. <https://doi.org/10.1007/s10853-009-3561-1>

33. Zhao TK, Hou CL, Zhang HY et al (2014) Electromagnetic wave absorbing properties of amorphous carbon nanotubes. *Sci Rep* 4:5619. <https://doi.org/10.1038/srep05619>
34. Yang Y, Li M, Wu Y, Zong B, Ding J (2016) Size-dependent microwave absorption properties of Fe₃O₄ nanodiscs. *RSC Adv* 6:25444. <https://doi.org/10.1039/C5RA28035D>
35. Pandey S, Jana KK, Aswal VK, Rana D, Maiti P (2017) Effect of nanoparticle on the mechanical and gas barrier properties of thermoplastic polyurethane. *Appl Clay Sci* 146:468. <https://doi.org/10.1016/j.clay.2017.07.001>
36. Bhattacharyya S, Ghosh S, Chaurasiya D, Srivastava KV (2015) Bandwidth-enhanced dual-band dual-layer polarization-independent ultra-thin metamaterial absorber. *Appl Phys A* 118:207. <https://doi.org/10.1007/s00339-014-8908-z>
37. Bhattacharyya R, Jha DK, Prakash O, Singh AP, Bhattacharyya S, Das S (2017) Ultra-thin ferrite nanocomposite coating as broad-band microwave absorber. In: 2017 IEEE applied electromagnetics conference (AEMC)
38. Bhattacharyya S, Ghosh S, Vaibhav Srivastava K (2013) Triple band polarization-independent metamaterial absorber with bandwidth enhancement at x-band. *J Appl Phys* 114:094514. <https://doi.org/10.1063/1.4820569>
39. Bhattacharyya S, Vaibhav Srivastava K (2014) Triple band polarization-independent ultra-thin metamaterial absorber using electric field-driven LC resonator. *J Appl Phys* 115:064508. <https://doi.org/10.1063/1.4865273>
40. Mashuri X, Lestari W, Triwikantoro X, Darminto X (2018) Preparation and microwave absorbing properties in the X-band of natural ferrites from iron sands by high energy milling. *Mater Res Express* 5(1):014003
41. Ohlan A, Singh K, Gandhi N, Chandra A, Dhawan SK (2011) Microwave absorption properties of NiCoFe₂O₄-graphite embedded poly(o-phenetidine) nanocomposites. *AIP Adv* 1:032157. <https://doi.org/10.1063/1.3642603>
42. Luo J, Zuo Y, Shen P, Yan Z, Zhang K (2017) Excellent microwave absorption properties by tuned electromagnetic parameters in polyaniline-coated Ba_{0.9}La_{0.1}Fe_{11.9}Ni_{0.1}O₁₉/reduced graphene oxide nanocomposites. *RSC Adv* 7:36433. <https://doi.org/10.1039/C7RA06800J>